Communications on Applied Nonlinear Analysis
ISSN: 1074-133X
Vol 31 No. 8s (2024)

Thermal Radiation, Chemical Reaction, Soret, Hall and Ion Slip Effects on Unsteady MHD Rotating Flow of Micropolar-Casson Fluid through Porous Medium

Suchita T.S [1], S Senthamilselvi[1], R. VijayaKumar[2] and A Jancy Rani[3]

[1]Department of Mathematics, Vels Institute of Science, Technology & Advanced Studies, Tamil Nadu, India.

[2]Mathematics Section,FEAT,Annamalai University, Annamalainagar-608002,India. Department of Mathematics, Periyar Government Arts College, Cuddalore, TamilNadu – 607 001, India.

[3]Department of Mathematics, Annamali University, Annamalainagar, Tamil Nadu- 608 002, India.

Email: *[1]chiku2712@gmail.com, [2]rathirath_viji@yahoo.co.in, [3]jancyrani1985@gmail.com*

Corresponding author Email: [1]msselvi2305@gmail.com

Article History:

Received: 22-06-2024

Revised: 15-07-2024

Accepted: 20-08-2024

Abstract:

The effects of heat radiation, chemical reaction, Hall and ion slip, as well as a flow of a fluid in which each particle moves along its line of flow with constant speed and in which the cross section of each stream tube remains unchanged transverse magnetic field and convective boundary conditions, on an unstable MHD natural convective rotating flow of micro-polar Casson fluid through extending to infinity in one direction the porous plate moving vertically have been studied. The boundary layer solutions must satisfy the no slip criterion since it is presumed that the entire system would vary in time by constant frequency. The perturbation approach is applied to solve the dimensionless governing equations analytically, and the outcomes are then computationally analysed to the relevant parameters by references. Heat and mass transfer which involves several natural and man-made transport systems on MHD flows across porous medium through chemical reactions. Hall and ion slip impacts are often exploited in the bio-medical field.

Keywords: Hall and ion slip impacts, Thermal radiation, Micropolar – Casson fluid, Rotating frame, Chemical reaction.

1. Introduction

Hari R [1] found an analytical solution to the unstable free convective MHD is studied. In the occurrence of chemical reaction, heat generation, ramped wall temperature, and ramped surface concentration with embedded porous medium, Casson fluid movement passed over an exponentially accelerated perpendicular plate. The Hall and Ion slip impacts on MHD rotating convective boundary layer flow of a nano-fluid through a semi-infinite horizontal permeable porous plate were designed by M. Veerakirishna[2]. Heat and mass transfer on MHD oscillatory flow through an lop-sided wavy channel examined by J. Sasikumar [3] through porous channel with suction and injection. Abdul Rahman Mohd Kasim [4] concentrated on the issue of fixed two-dimensional convective movement of a Casson fluid while also taking into account the microrotation impact over a stretch surface and mixed convection as the basis of heat transmission. The impacts of nanoparticle geometry, slip, and temperature wall circumstances on the thermo-magneto-solvent flow of nano fluid among two

parallel discs contained in a porous media have been rationally explored, as predicted by M. G. Sobamowo [5]. According to Dhananjay Yadav [6], the collective effect of temperature-dependent viscosity and an inside heat source on the beginning of convection in porous inserts saturated with a viscoelastic fluid has been investigated by means of linear and weak nonlinear stability models. Sara I [7] looked examined the mathematical outcomes of peristaltic transportation of a blood as non-Newtonian through a ununiform channel in the presence of an exterior magnetic field, a concentration of nanoparticles, a chemical reaction, a Hall current, and ion slip. In the occurrence of chemical processes and thermal radiation, Omar T. Bafakeeh [8] predicted the unsteady MHD free convection movement of a viscous, incompressible, and electrically conducting flowing over a perpendicular plate embedded in a porous media. The main and secondary flows of a micropolar fluid through an inclined plate with viscous dissipation and thermal radiation were investigated by M.D. Shamshuddin [9] in a rotating frame. Hall and ion-slip effects were taken into consideration when M. Veera Krishna [10] studied the steady MHD laminar flow of an elastico-viscous, electrically conducting Walter's B fluid through a spherical cylinder or pipe that is loosely packed with porous material. M. Veera Krishna [11] calculated the effects of angle of inclination, changing temperature, and concentration on the Hall and ion slip effects on the unsteady MHD free convective flow across an exponentially accelerating inclined plate embedded in a saturated porous media. M. Veera Krishna [12] studied the effects of uniform transverse magnetic field, convective boundary conditions, thermal radiation, chemical reaction, Hall, and ion-slip on convection by two different level density with different rate diffusion (double-diffusive) unstable MHD natural convective rotating flow of micropolar fluid through extending to infinity in one direction vertically moving porous plate. Dhananjay Yadav [13] investigated the issue of convective instability for an electrically conducting nanofluid layer under magnetic field with a physically more realistic boundary condition on the volumetric fraction of nanoparticles, i.e., by assuming that the flux of nanoparticles is zero rather than imposing the volumetric fraction of nanoparticles on rigid boundaries. According to M. Veera Krishna [14], the effects of Hall and ion slip on the MHD convective flow of elastico-viscous fluid through a porous media between two rigidly rotating parallel plates with a time-varying sinusoidal pressure gradient were studied. D. Srinivasacharya [15]looks at how the magnetic field affects the mixed convective flow of nano fluid between the annuli of two concentric co-axial cylinders using the characteristics of thermophoresis, Brownian motion, Hall, and ion slip. In this research, Dulal Pala [16] looks at the impact of thermal radiation and chemical reaction on the double- diffusive convective heat and mass transfer of MHD oscillatory flow of a micropolar fluid across a vertical plate embedded in a porous medium with convective boundary conditions. Muhammad Sohail [17] used a theoretical and numerical technique to analyze MHD three-dimensional boundary layer movement of a steady incompressible Casson fluid through a rectilinear stretchy surface with Cattaneo-Christov convection by two different level density with different rate diffusion (double diffusion). The unsteady natural convection flow of a rotating fluid over and done with an exponentially accelerated perpendicular plate with Hall current, ion-slip, and magnetic effect is examined by Jitendra Kumar Singh [18].

From all the aforementioned, Hall, and ion slip impacts with thermal radiation and chemical reaction on the convection by two different level density with different rate diffusion (double-diffusive) unsteady MHD natural convective rotating flow of micro-polar Casson fluid over and done with a

semi-infinite perpendicular porous wavy channel through convective boundary conditions has not been yet discussed. Thus, it has been planned to examine the impacts of thermal radiation, chemical reaction, Soret with Hall and Ion slip effects, and convective boundary conditions on unsteady MHD natural convective rotating flow of micro-polar Casson fluid over and done with a semi-infinite perpendicular moving porous plate.

2. Mathematical Formulation

The consequences of thermal diffusivity, chemical reaction, Hall impacts, and ion slip are measured. The investigation is done with the impact of a diagonal magnetic field and convective boundary conditions on incompressible an unstable free convective hydromagnetic Micropolar - Casson fluid flow confined through extending to infinity in one direction in porous plate within a rotating frame. The wavy channel one side wall $z = h' = d + a\cos\lambda x$ at z=h .In this case, the effects of Soret, chemical reactions, Hall, and ion slip impacts are considered.

- The occurrence of heat and concentration buoyancy forces causes a uniform transverse magnetic field B_0 to impose on the flow motion.
- Initial and uninterrupted condition, micropolar Casson fluid and plate have been rigidly rotating by means of the same angular velocity with respect to the normal to the plate.
- As seen in Figure 1, the z-axis is at right angles to the x-axis and is taken into account with the plate in the vertical direction.
- The applied magnetic field dominates over the magnetic field that is induced. The magnetic field is considered to have a lower density.
- The fluid is said to be Gray and to either emit or absorb radiation.
- The Rosseland approximation is applied to represent the radiative heat flux in the z-direction.
- The plate moves up along its own plane constantly and uniformly.
- It is expected that the surface temperature will remain constant at Tw even though the ambient temperature take hold off on the constant value T, resulting in the relationship Tw > T.
- Concentration close to the boundary surface be consistently considered as Cw, while ambient fluid concentration be taken as C.

The boundary layer equations for motion, energy, and mass diffusion in the presence of a uniform transverse magnetic field and the frequency of thermal diffusion and chemical reaction remained as follows under these presumptions.

The flow of governing equations [12]

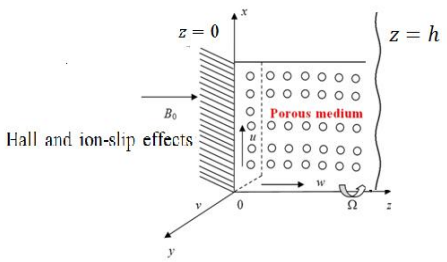

Figure 1: Physical model of the problem

Governing Equations

$$\frac{\partial w}{\partial z} = 0$$
(1)

$$\frac{\partial u}{\partial t'} + w\frac{\partial u}{\partial z} - 2\Omega v = \left(\nu\left(1+\frac{1}{\beta'}\right)+\nu_r\right)\frac{\partial^2 u}{\partial z^2} + \frac{B_0 J_y}{\rho} - \frac{\nu+\nu_r}{k}u + g\beta_T(T-T_1) + g\beta_C(C-C_1) - 2\nu_r\frac{\partial \omega_2^*}{\partial z} \quad (2)$$

$$\frac{\partial v}{\partial t'} + w\frac{\partial v}{\partial z} + 2\Omega u = \left(\nu\left(1+\frac{1}{\beta'}\right)+\nu_r\right)\frac{\partial^2 v}{\partial z^2} - \frac{B_0 J_x}{\rho} - \frac{\nu+\nu_r}{k}v + 2\nu_r\frac{\partial \omega_1^*}{\partial z} \quad (3)$$

$$\frac{\partial \omega_1^*}{\partial t'} + w\frac{\partial \omega_1^*}{\partial z} = \frac{\gamma}{\rho_j}\frac{\partial^2 \omega_1^*}{\partial z^2} \quad (4)$$

$$\frac{\partial \omega_2^*}{\partial t'} + w\frac{\partial \omega_2^*}{\partial z} = \frac{\gamma}{\rho_j}\frac{\partial^2 \omega_2^*}{\partial z^2} \quad (5)$$

$$\frac{\partial T}{\partial t'} + w\frac{\partial T}{\partial z} = \alpha\frac{\partial^2 T}{\partial z^2} - \frac{1}{\rho C_p}\frac{\partial q_r}{\partial z} \quad (6)$$

$$\frac{\partial C}{\partial t'} + w\frac{\partial C}{\partial z} = D\frac{\partial^2 C}{\partial z^2} + K_r^*(C-C_1) + D_1\frac{\partial^2 T}{\partial z^2} \quad (7)$$

The boundary conditions are described by,

$$t<0 \quad u=v=0,\ T=T_1,\ C=C_1, \omega_1^*=0\ \omega_2^*=0 \quad , \quad (8)$$

$$t>0 \quad u=\frac{\sqrt{K_p}}{\alpha_f}\frac{\partial u}{\partial z},$$

$$v=0,\ -K_T\frac{\partial T}{\partial z}=\alpha_h(T_1-T),\ -K_C\frac{\partial C}{\partial z}=\alpha_m(C_1-C), \omega_1^*=\frac{-i}{2}\frac{\partial v}{\partial z}, \omega_2^*=\frac{i}{2}\frac{\partial v}{\partial z} \quad \text{at} \quad z=0$$

$$u=\frac{-\sqrt{K_p}}{\alpha_f}\frac{\partial u}{\partial z},\ v=0,\ -K_T\frac{\partial T}{\partial z}=\alpha_h(T-T_2),\ -K_C\frac{\partial C}{\partial z}=\alpha_m(C-C_2), \omega_1^*=\frac{-i}{2}\frac{\partial v}{\partial z}, \omega_2^*=\frac{i}{2}\frac{\partial v}{\partial z} \quad \text{at} \quad z=h$$
(9)

The continuity Eq. (1) makes the suction velocity clear and it is only useful in terms of time, hence it might be expressed as the following formula[19].

$$w = -w_0(1+\varepsilon A e^{nt}) \quad (10)$$

Where A an existing positive invariable, $\varepsilon A << 1$adding to $w_0$be a magnitude of suction velocity in which $w_0 > 0$. β'-Casson parameter, g-acceleration, D-mass diffusivity, ρ-density, β_T –coefficient of volume expansion, β_C - coefficient of volume expansion with concentration-kinematic viscosity, K_r*-absorption coefficient,D_1-thermal diffusion coefficient, k-permeability of porous medium,α-thermal conductivity,C_p-specific heat at constant pressure,

Choose the radiative heat flow, q_r, in the fluid medium before moving on. The Rosseland approximation will be used to estimate this term in the current study[20].

$$q_r = -\frac{4\sigma}{3k_2}\frac{\partial T^4}{\partial z} \quad (11)$$

Considering that the flow is surrounded by a temperature different, then the linear combination of temperature$T^4$is defined. Developing T^4 by Tayler's series tends to T_∞ as of the following,

$$T^4 = T_\infty^4 + 4T_\infty^3(T - T_\infty) + 6T_\infty^2(T - T_\infty)^2 + \cdots, \quad (12)$$

Ignoring higher order expressions forward to the foremost degree within $(T - T_\infty)$,

$$T^4 \approx -3T_\infty^4 + 4T_\infty^3 T \quad (13)$$

with respect to z, differentiate the equation (12) and making use the equation (13)

$$\frac{\partial q_r}{\partial z} = -\frac{16T_\infty^3}{3k_2}\frac{\partial^2 T}{\partial z^2} \quad (14)$$

Since the frequency of electron-atom collisions is speculated to be quite high, hall and ion slip effects cannot be ignored. Consequently, the velocity is produced by the hall and ion slip currents. The hall and ion slip effect be added to the generalized ohm's law once the magnetic field strength is actually strong.

$$J = \sigma(E + V \times B) - \frac{\omega_e\tau_e}{B_0}(J \times B) + \frac{\omega_e\tau_e\beta_i}{B_0^2}\big((J \times B) \times B\big) \quad (15)$$

Additionally, $\beta_e = \omega_e\tau_e \approx O(1)$be the hall parameter and $\beta_i = \omega_i\tau_i << 1$be the ion slip parameter in the equation (15), the electron pressure gradient and thermoelectric impacts are ignored, particularly, the electric field $E = 0$, by means of these assumptions, the equation (15) condensed to component methods as,

$$(1 + \beta_i\beta_e)J_x + \beta_e J_z = \sigma B_0 v \quad (16)$$

$$(1 + \beta_i\beta_e)J_z - \beta_e J_x = -\sigma B_0 u \quad (17)$$

where, $\beta_e = \omega_e\tau_e$be the parameter of hall effect. Resolving the equations (16) and (17),

$$J_x = \sigma B_0(\alpha_2 u + \alpha_1 v) \quad (18)$$

$$J_z = -\sigma B_0(\alpha_2 v - \alpha_1 u) \quad (19)$$

Where,

$$\alpha_1 = \frac{1 + \beta_e\beta_i}{(1 + \beta_e\beta_i)^2 + \beta_e^2},$$

$$\alpha_2 = \frac{\beta_e}{(1+\beta_e\beta_i)^2+\beta_e^2}$$

Replacing the equations (18) – (19) in (3) – (2) accordingly, we obtain

$$\frac{\partial u}{\partial t'} + w\frac{\partial u}{\partial z} - 2\Omega v = \left(\nu\left(1 + \frac{1}{\beta'}\right) + \nu_r\right)\frac{\partial^2 u}{\partial z^2} + \frac{\sigma B_0^2(\beta_I v + \beta_{II} u)}{\rho} - \frac{\nu + \nu_r}{k}u$$
$$+ g\beta_T(T - T_1) + g\beta_C(C - C_1) - 2\nu_r\frac{\partial \omega_2^*}{\partial z} \quad (20)$$

$$\frac{\partial v}{\partial t'}+w\frac{\partial v}{\partial z}-2\Omega u=\left(\nu\left(1+\frac{1}{\beta'}\right)+\nu_r\right)\frac{\partial^2 v}{\partial z^2}-\frac{\sigma B_0^2(\beta_I u+\beta_{II}v)}{\rho}-\frac{\nu+\nu_r}{k}v+2\nu_r\frac{\partial\omega_1^*}{\partial z} \quad (21)$$

Exhibiting homogeneity and non-dimensional quantities in the following,

$$U=\frac{u}{w_0},\ V=\frac{v}{w_0},\ W=\frac{w}{w_0},\ z'=\frac{z}{d},\ t=\frac{t'w_0}{d},\ \eta'=\frac{\eta d}{w_0},\quad \theta=\frac{(T-T_1)}{T_2-T_1},\varphi=\frac{(C-C_1)}{C_2-C_1},$$
$$\omega_1=\frac{\omega_1^* d}{w_0},\omega_2=\frac{\omega_2^* d}{w_0},h=\frac{h'}{d}$$

$\beta_r=\frac{\Lambda}{\mu}=\frac{\nu_r}{\nu}$–Dimensionless viscosity ratio, $R=\frac{\Omega d^2}{\nu}$– Rotation Parameter, $M^2=\frac{B_0\sigma d}{w_0\rho}$–Hartmann number, $Pr=\frac{\nu}{K_r}$ – Prandtl number, $Sc=\frac{\nu}{D}$–Schmidt number, $K=\frac{k}{d^2}$–Permeability Parameter, $Sr=\frac{D_1(T_2-T_1)}{\nu(C_2-C_1)}$–Soret number, $Gr=\frac{g\beta_T\nu(T_2-T_1)}{w_0^3}$ – Thermal Grashof number, $Gm=\frac{g\beta_T\nu(C_2-C_1)}{w_0^3}$ – Mass Grashof number, $\delta=\frac{\nu_1}{\rho_j}$–Material Parameter, $N=\frac{4\sigma^*T_1^3}{k_1k_2}$ – Radiation Parameter, $Kc=\frac{\nu kc}{w_0^2}$– Chemical reaction Parameter.

The governing equations (20), (21), (4) – (7) reduced by using of Non – dimensional variables to the following

$$\frac{\partial u}{\partial t}-(1+\varepsilon Ae^{nt})\frac{\partial u}{\partial z'}-2Rv=\left[\left(1+\frac{1}{\beta'}\right)+\beta_r\right]\frac{\partial^2 u}{\partial z'^2}+M^2(\beta_I v+\beta_{II}u)-\left(\frac{1+\beta_r}{K}\right)u$$
$$+Gr\theta+Gm\varphi-2\beta_r\frac{\partial\omega_2}{\partial z'} \quad (22)$$

$$\frac{\partial v}{\partial t}-(1+\varepsilon Ae^{nt})\frac{\partial v}{\partial z'}+2Ru=\left[\left(1+\frac{1}{\beta'}\right)+\beta_r\right]\frac{\partial^2 v}{\partial z'^2}-M^2(\beta_I u+\beta_{II}v)$$
$$-\left(\frac{1+\beta_r}{K}\right)v+2\beta_r\frac{\partial\omega_1}{\partial z'} \quad (23)$$

$$\frac{\partial\omega_1}{\partial t}-(1+\varepsilon Ae^{nt})\frac{\partial\omega_1}{\partial z'}=\frac{1}{\delta}\frac{\partial^2\omega_1}{\partial z'^2} \quad (24)$$

$$\frac{\partial\omega_2}{\partial t}-(1+\varepsilon Ae^{nt})\frac{\partial\omega_2}{\partial z'}=\frac{1}{\delta}\frac{\partial^2\omega_2}{\partial z'^2}$$
(25)

$$\frac{\partial\theta}{\partial t}-(1+\varepsilon Ae^{nt})\frac{\partial\theta}{\partial z'}=\frac{1}{Pr}\left(1+\frac{4N}{3}\right)\frac{\partial^2\theta}{\partial z'^2} \quad (26)$$

$$\frac{\partial\varphi}{\partial t}-(1+\varepsilon Ae^{nt})\frac{\partial\varphi}{\partial z'}=\frac{1}{Sc}\frac{\partial^2\varphi}{\partial z'^2}+Kc\varphi+Sr\frac{\partial^2\theta}{\partial z'^2} \quad (27)$$

Applicable boundary conditions be,

$$t < 0 \quad q = 0 \quad T = 0 \quad C = 0 \quad \omega_1 = 0 \; \omega_2 = 0 \tag{28}$$

$$t > 0, \frac{\partial q}{\partial z'} = \alpha_f \sigma q, \frac{\partial \theta}{\partial z'} = B_h \theta, \; \frac{\partial \varphi}{\partial z'} = B_m \varphi, \; \omega_1 = \frac{-1}{2}\frac{\partial q}{\partial z'}, \quad \omega_2 = 0 \text{ at } z' = 0 \tag{29}$$

$$\frac{\partial q}{\partial z'} = -\alpha_f \sigma q, \; \frac{\partial \theta}{\partial z'} = B_h(1-\theta), \; \frac{\partial \varphi}{\partial z'} = B_m(1-\varphi), \; \omega_1 = \frac{-1}{2}\frac{\partial q}{\partial z'}, \quad \omega_2 = 0 \text{ at } \; z' = h$$

Combining the equations (22) and (23); (24) and (25),

Let $q = u + iv$ and $\omega = \omega_1^* + i\omega_2^*$, we acquired,

$$\frac{\partial q}{\partial t} - (1 + \varepsilon A e^{nt})\frac{\partial q}{\partial z'} = \left(\left(1 + \frac{1}{\beta'}\right) + \beta_r\right)\frac{\partial^2 q}{\partial z'^2} - \left(M^2(\beta_I v + \beta_{II} u) + \frac{1+\beta_r}{K} + 2iR\right)q + Gr\theta + Gm\varphi + 2i\beta_r \frac{\partial \omega}{\partial z'}$$

(30)

$$\frac{\partial \omega}{\partial t} - (1 + \varepsilon A e^{nt})\frac{\partial \omega}{\partial z'} = \frac{1}{\delta}\frac{\partial^2 \omega}{\partial z'^2}$$

(31)

3. Method of Solution

Assume the perturbation approach to acquire the solutions of the beyond scheme of partial differential equalities (dropping the apostrophe) (30-31) and (26-27) under the pertinent boundary conditions.

$$q(z,t) = q_0(z) + \varepsilon e^{i\omega t} q_1(z) + O(\varepsilon^2) \tag{32}$$

$$\omega(z,t) = \omega_0(z) + \varepsilon e^{i\omega t} \omega_1'(z) + O(\varepsilon^2) \tag{33}$$

$$\theta(z,t) = \theta_0(z) + \varepsilon e^{i\omega t} \theta_1(z) + O(\varepsilon^2) \tag{34}$$

$$\varphi(z,t) = \varphi_0(z) + \varepsilon e^{i\omega t} \varphi_1(z) + O(\varepsilon^2) \tag{35}$$

The following set of equations were attained by substituting equations (32) to (35) into equations (26), (27), (30) and (31), while absorbing the harmonic and non-hormonic terms and ignoring the higher power terms of $O(\varepsilon^2)$:

Zeroth order Equations

$$f_{30}\frac{\partial^2 q_0}{\partial z^2} + \frac{\partial q_0}{\partial z} - f_{290} q_0 = -Gr\theta_0 - Gm\varphi_0 + 2i\beta_r \frac{\partial \omega_0}{\partial z} \tag{36}$$

$$\frac{\partial^2 \omega_0}{\partial z^2} + \delta \frac{\partial \omega_0}{\partial z} = 0 \tag{37}$$

$$\frac{\partial^2 \theta_0}{\partial z^2} + f_1 \frac{\partial \theta_0}{\partial z} = 0 \tag{38}$$

$$\frac{\partial^2 \varphi_0}{\partial z^2} + Sc\frac{\partial \varphi_0}{\partial z} - Kr\, Sc\, \varphi_0 = -Sc\frac{\partial^2 \theta_0}{\partial z^2} \tag{39}$$

The corresponding boundary conditions are as follows

$$\frac{\partial q_0}{\partial z} = \alpha_f \sigma q_0, \frac{\partial \theta_0}{\partial z} = B_h \theta_0, \; \frac{\partial \varphi_0}{\partial z} = B_m \varphi_0, \; \omega_0 = \frac{-1}{2}\frac{\partial q_0}{\partial z} \qquad \text{at z=0}$$

$\frac{\partial q_0}{\partial z} = -\alpha_f \sigma q_0,\ \frac{\partial \theta_0}{\partial z} = B_h(1-\theta_0),\ \frac{\partial \varphi_0}{\partial z} = B_m(1-\varphi_0),\ \omega_0 = 0$ at z=h

Solving the equations (36) to (39) under the boundary conditions, we obtain the velocity, temperature, concentration and microrotation

$$q_0 = A_{15}e^{m_9 z} + A_{16}e^{m_{10} z} + f_{34}Sin[f_1 z] + f_{35}Cos[f_1 z] + f_{36}e^{m_3 z} + f_{37}e^{m_4 z} + f_{38}A_{10}e^{-\delta z}$$

$$\omega_0 = A_9 + A_{10}e^{-\delta z}$$

$$\theta_0 = A_1 \cos[f_1 z] + A_2 \sin[f_1 z]$$

$$\varphi_0 = A_5 e^{m_3 z} + A_6 e^{m_4 z} + f_{13}\sin[f_1 z] + f_{14}\cos[f_1 z]$$

First order Equations

$$f_{30}\frac{\partial^2 q_1}{\partial z^2} + \frac{\partial q_1}{\partial z} - \left(in + f_{290}\right) = -A\frac{\partial q_0}{\partial z} - Gr\theta_1 - Gm\varphi_1 + 2i\beta_r\frac{\partial \omega_1'}{\partial z} \quad (40)$$

$$\frac{\partial^2 \omega_1'}{\partial z^2} + \delta\frac{\partial \omega_1'}{\partial z} - in\delta\omega_1' = -A\frac{\partial \omega_0}{\partial z}\delta \quad (41)$$

$$\frac{\partial^2 \theta_1}{\partial z^2} + f_1\frac{\partial \theta_1}{\partial z} - inf_1\theta_1 = -Af_1\frac{\partial \theta_0}{\partial z} \quad (42)$$

$$\frac{\partial^2 \varphi_1}{\partial z^2} + Sc\frac{\partial \varphi_1}{\partial z} - (Kr - in)\varphi_1 = -A\,Sc\frac{\partial \varphi_0}{\partial z} - Sr\,Sc\frac{\partial^2 \theta_1}{\partial z^2} \quad (43)$$

The corresponding boundary conditions are as follows

$\frac{\partial q_1}{\partial z} = \alpha_f \sigma q_1,\ \frac{\partial \theta_1}{\partial z} = B_h\theta_1,\ \frac{\partial \varphi_1}{\partial z} = B_m\varphi_1,\quad \omega_1' = \frac{-1}{2}\frac{\partial q_1}{\partial z},$ at z=0

$\frac{\partial q_1}{\partial z} = -\alpha_f \sigma q_1, \frac{\partial \theta_1}{\partial z} = -B_h\theta_1,\ \frac{\partial \varphi_1}{\partial z} = B_m\varphi_1,\ \omega_1' = 0,$ at z=h

Solving the equations (40) to (43) under the boundary conditions, we obtain the velocity, temperature, concentration and microrotation

$$\begin{aligned} q_1 = {} & A_{13}e^{m_{11} z} + A_{14}e^{m_{12} z} + f_{41}e^{m_9 z} + f_{42}A_{11}e^{m_{10} z} + f_{43}A_{12}Sin[f_1 z] + f_{44}Cos[f_1 z] \\ & + f_{45}e^{m_3 z} + f_{46}e^{m_4 z} + A_{10}f_{47}e^{-\delta z} + f_{48}e^{m_1 z} + f_{49}e^{m_2 z} + f_{50}e^{m_5 z} + f_{51}e^{m_6 z} \\ & + f_{52}A_{11}e^{m_7 z} + f_{53}A_{12}e^{m_8 z} \end{aligned}$$

$$\omega_1' = A_{11}e^{-m_7 z} + A_{12}e^{8z} + f_{29}e^{-\delta z}$$

$$\theta_1 = A_3 e^{m_1 z} + A_4 e^{m_2 z} + f_6\cos[f_1 z] + f_7\sin[f_1 z]$$

$$\varphi_1 = A_7 e^{m_5 z} + A_8 e^{m_6 z} + f_{23}e^{m_8 z} + f_{24}e^{m_4 z} + f_{25}e^{m_1 z} + f_{26}e^{m_2 z} + f_{27}\cos[f_1 z] + f_{28}\sin[f_1 z]$$

solutions for the following equations with respect to velocity, microrotation, temperature, and concentration are:

$$\begin{aligned} q = {} & A_{15}e^{m_9 z} + A_{16}e^{m_{10} z} + f_{34}Sin[f_1 z] + f_{35}Cos[f_1 z] + f_{36}e^{m_3 z} + f_{37}e^{m_4 z} + f_{38}A_{10}e^{-\delta z} \\ & + \varepsilon e^{i\omega t}\left(A_{13}e^{m_{11} z} + A_{14}e^{m_{12} z} + f_{41}e^{m_9 z} + f_{42}A_{11}e^{m_{10} z} + f_{43}A_{12}Sin[f_1 z]\right. \\ & + f_{44}Cos[f_1 z] + f_{45}e^{m_3 z} + f_{46}e^{m_4 z} + A_{10}f_{47}e^{-\delta z} + f_{48}e^{m_1 z} + f_{49}e^{m_2 z} + f_{50}e^{m_5 z} \\ & \left. + f_{51}e^{m_6 z} + f_{52}A_{11}e^{m_7 z} + f_{53}A_{12}e^{m_8 z}\right) \end{aligned}$$

$$\omega = A_9 A_{10} e^{-\delta z} + \varepsilon e^{i\omega t}\left(A_{11} e^{-m_7 z} + A_{12} e^{8z} + f_{29} e^{-\delta z}\right)$$

$$\theta = A_1 \cos[f_1 z] + A_2 \sin[f_1 z] + \varepsilon e^{i\omega t}(A_3 e^{m_1 z} + A_4 e^{m_2 z} + f_6 \cos[f_1 z] + f_7 \sin[f_1 z])$$

$$\varphi = A_5 e^{m_3 z} + A_6 e^{m_4 z} + f_{13} \sin[f_1 z] + f_{14} \cos[f_1 z] + \varepsilon e^{i\omega t}(A_7 e^{m_5 z} + A_8 e^{m_6 z} + f_{23} e^{m_3 z} + f_{24} e^{m_4 z} + f_{25} e^{m_1 z} + f_{26} e^{m_2 z} + f_{27} \cos[f_1 z] + f_{28} \sin[f_1 z])$$

Skin friction, Nusselt number, and Sherwood number in dimensional form at the plate are,

$\tau = \left(\frac{\partial q}{\partial z}\right)$ at $z = 0$,h

$Nu = -\left(\frac{\partial \theta}{\partial z}\right)$ at $z = 0$,h

$Sh = -\left(\frac{\partial \psi}{\partial z}\right)$ at $z = 0$,h

4. Result and Discussion

The effects of Hall, and ion slip with thermal radiation, chemical reaction on an unsteady MHD natural convective rotating flow of micro-polar Casson fluid surrounded through a semi-infinite perpendicular moving porous plate have been taken into consideration by the influence of a uniform transverse magnetic field and boundary conditions. Some fixed values were set with the intention of calculating certain components $N = 1$, $Kc = 4$, $\epsilon = 0.5$, $Sc = 0.78$, $Bh = 0.4$, $Bm = 0.1$, $Sr = 0.5$, $Pr = 7$, $\delta = 1$, $K = 0.5$, $M = 1$, $\beta' = 1$, $\beta r = 0.5$, $R = 1.5$, $t = 1$, $Gr = 1$, $Gm = 6$, $A = 1$, $D_1 = 0.5$, $\sigma = 0.5$, $\alpha_e = 0.4$, $\alpha_i = 2$.

Figure 2 demonstrated that the Hartmann number (M) characterizes magnetic field strength in a conducting fluid and the fluid motion and altering the velocity profile can be interacted. Magnetic field effect is stronger in regions of high velocity, where the Lorentz force is larger. As a result, the velocity profile becomes flatter and broader in the presence of a magnetic field. This effect can be quantified by the Hartmann number (M), which is a measure of the ratio between the Lorentz force and the viscous force in the fluid. Therefore, as the Hartmann number (M) increases, the strength of the magnetic field becomes stronger relative to the fluid viscosity, more significant reduction in resulting velocity and a broader, flatter velocity profile in both the U and V regions.

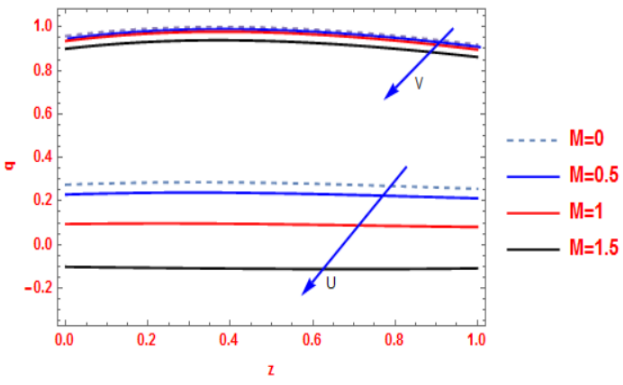

Figure 2 The velocity profile against M

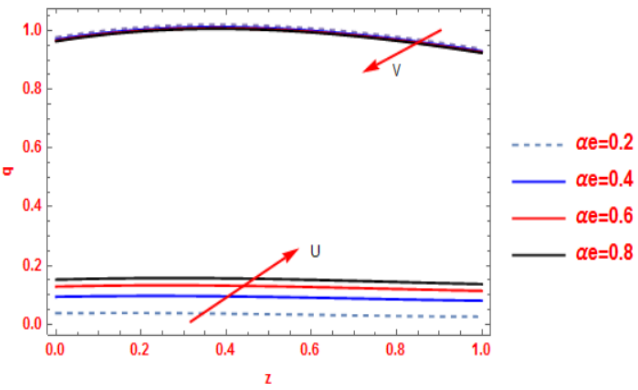

Figure 3 The velocity profile against α_e

In the context of a velocity profile, figure 3 that the Hall parameter (α_e)augments in the region U and lessens in the region V because of the effect of the magnetic field on the fluid. When the fluid flows through the region U, it experiences a strong magnetic field, which causes it to slow down due to the Lorentz force. This results in a lessening in the velocity and a rise in the Hall parameter (α_e). the Hall parameter (α_e) is a measure of the relative strength of the magnetic field and the viscous forces in a flowing fluid. Its behavior in different regions of the velocity profile is determined by the local strength of the magnetic field and the viscosity of the fluid.

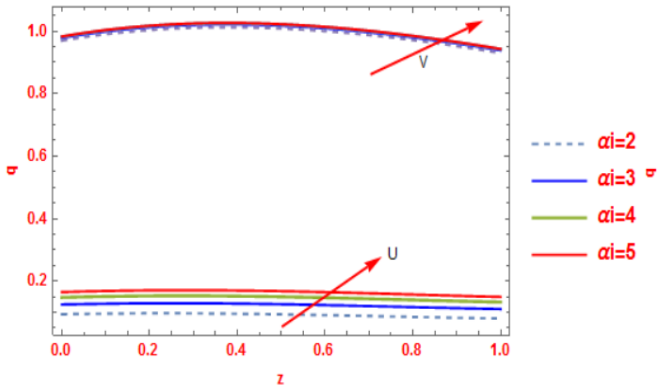

Figure 4 The velocity profile against α_i

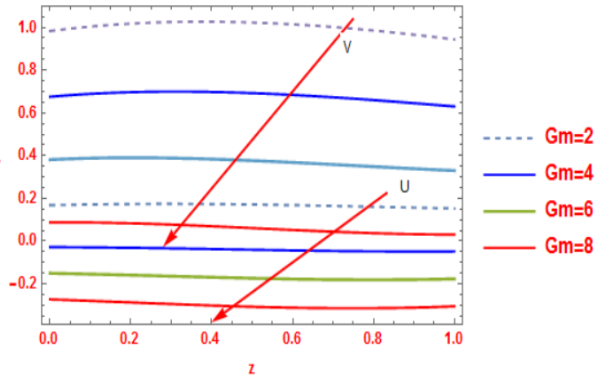

Figure 5 The velocity profile against Gm

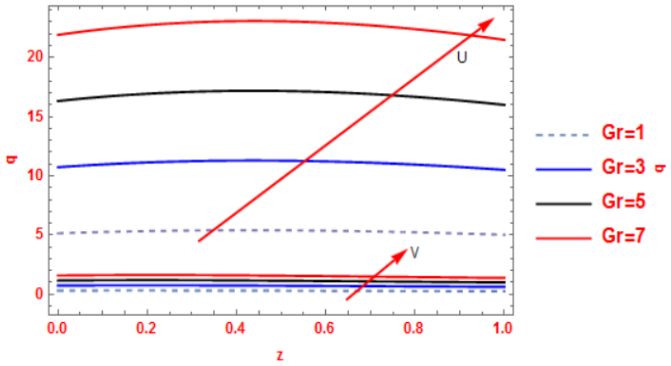

Figure 6 The velocity profile against Gr

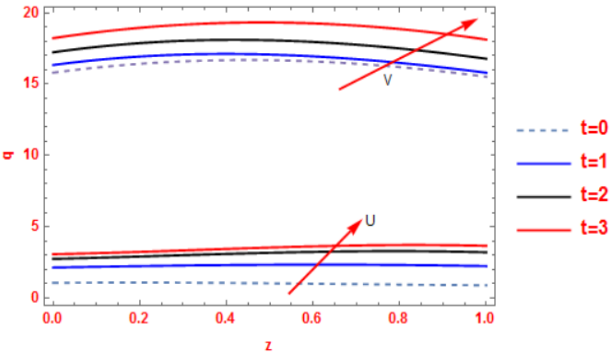

Figure 7 The velocity profile against (t)

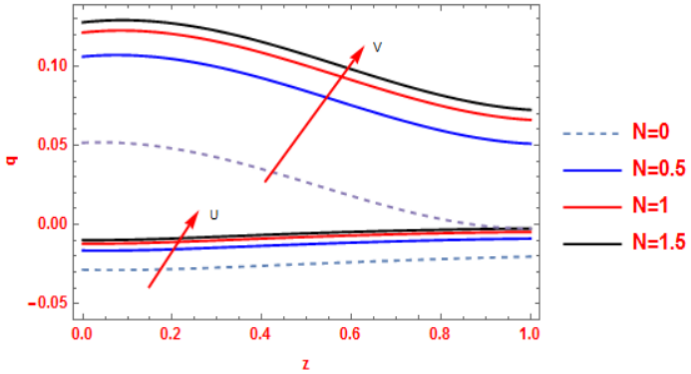

Figure 8 The velocity profile against N

Figure 4 that the ion slip parameter (α_i) is defined as the ratio of the ion gyrofrequency to the electron collision frequency. It is a dimensionless parameter that quantifies the importance of the Hall effect in a plasma. When the ion slip parameter (α_i) is large, the Hall effect is dominant and can significantly alter the plasma's velocity profile. Specifically, the ion slip parameter (α_i) can affect both the U and V regions of the velocity profile because it can create a shearing effect between these regions. The U region is typically characterized by a high ion density and a relatively low electron temperature, while the V region has a lower ion density and a higher electron temperature. When the ion slip parameter (α_i) is large, the Hall effect can cause a shearing between these regions, leading to a rise in the fluid velocity profile in both the U and V regions.

Figure 5 that the mass Grashof number(Gm) specifically takes into account the effects of density variations in the fluid. While the mass Grashof number (Gm) rises, the buoyancy force controls over the viscous force, leading to the development of convection currents in the fluid. These convection currents cause mixing and lead to aextra uniform temperature distribution within the fluid. As a result, the velocity profile becomes more uniform and the velocity in both regions U and V decreases.

Figure 6 that he thermal Grashof number (Gr) is well-defined in place of the product of the ratio, the forces of buoyancy to viscous Grashof number (Gr) and the thermal diffusivity ratio to kinematic viscosity (Pr). When the Grashof number (Gr) number increases, it implies that the buoyancy forces become relatively stronger than the viscous forces. As a result, the velocity profile in both the regions U and V is affected. In the region U (parallel to the hot surface), the velocity increases as the convective cells form and transport fluid particles upwards. In the region V (perpendicular to the hot surface), the velocity also increases due to the mixing and exchange of fluid particles caused by the convective cells. This leads to a more uniform velocity profile across the flow direction. Hence the increase in the thermal Grashof number (Gr) enhances the buoyancy-driven convection, which affects the velocity profile in both the U and V regions of the fluid flow.

Figure 7 that the dimensionless time (t), also known as the dimensionless variable, is a parameter used to describe the velocity profile over time as fluid flows through the channel. As the fluid flows through the channel, the velocity profile changes over time due to various factors such as friction, turbulence, and viscosity. In both the U and V regions of the velocity profile, the dimensionless time (t) increases because the fluid particles in these regions are moving at a slower velocity than in the core region. As the fluid flows through the channel, the velocity profile changes over time due to various factors such as friction, turbulence, and viscosity. In both the U and V regions of the velocity profile, the dimensionless time t increases because the fluid particles in these regions are moving at a slower velocity than in the core region. As the fluid particles in the U and V regions move at a slower velocity than those in the core region, it takes them more time to travel the same distance. This is why the dimensionless time (t) increases in both the U and V regions of the velocity profile.

Figure 8 that the radiation parameter (N) can affect the velocity profile of a fluid in multiple ways. Radiation parameter (N) represents the ratio of the radiation heat transfer to the convective heat transfer in the fluid. When (N)

increases, the importance of radiation heat transfer relative to convective heat transfer increases as well. One way in which this can affect the velocity profile is by altering the temperature gradient in the fluid.

Temperature Profile

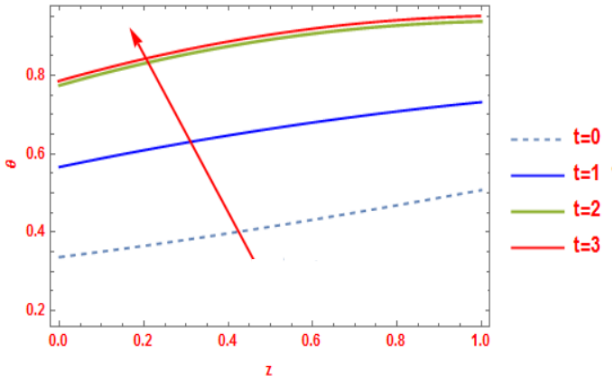

Figure 9 The temperature profile against t

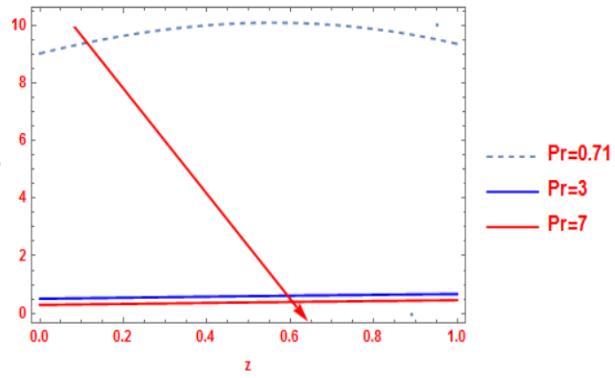

Figure 10 The temperature profile against Pr

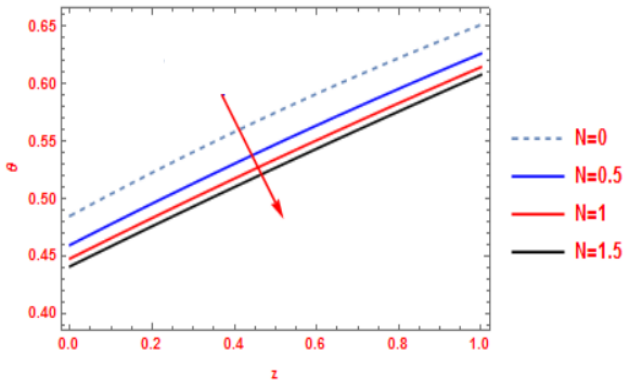

Figure 11 The temperature profile against N

Figure 9 that the temperature profile can be described using a dimensionless time (t) variable. dimensionless time (t) increases in the temperature profile are that it represents a normalized measure of time. Specifically, it is defined as the product of the physical time (t) and some scaling factor that depends on the specific physical system being studied. As time (t) increases, so does the dimensionless time (t), because the scaling factor remains constant. The increase in dimensionless time (t) in a temperature profile reflects the evolution of the temperature profile over time, normalized using a scaling factor that depends on the specific physical system being studied.

Figure 10 that the Prandtl number (Pr) relates the momentum diffusivity of a fluid to its thermal diffusivity and as the ratio of the kinematic viscosity to the thermal diffusivity of the fluid. Prandtl number (Pr) can decrease due to changes in the fluid properties as temperature changes. Typically, the thermal diffusivity of a fluid increases with temperature, while the kinematic viscosity of the fluid decreases with temperature. Hence the temperature increases, the ratio of the kinematic viscosity to the thermal diffusivity (i.e., the Prandtl number) will decrease.

Figure 11 that the Thermal radiation (N) is the emission of electromagnetic waves by a material due to its temperature. According to the Stefan-Boltzmann law, the amount of thermal radiation (N) emitted by a material is proportional to the fourth power of its absolute temperature. As the temperature of a material increases, the amount of thermal radiation (N) it emits increases significantly. However, in a temperature profile, the thermal radiation (N) parameter may appear to lessening as the temperature increases. This is because other factors can also influence the temperature profile, such as heat transfer through conduction or convection, which may increase the temperature more rapidly than the increase in thermal radiation (N). Hence while the amount of thermal radiation (N) emitted by a material increases with temperature according to the Stefan-Boltzmann law, other factors can affect the temperature profile and cause the thermal radiation (N) parameter to appear to decrease.

Concentration Profile

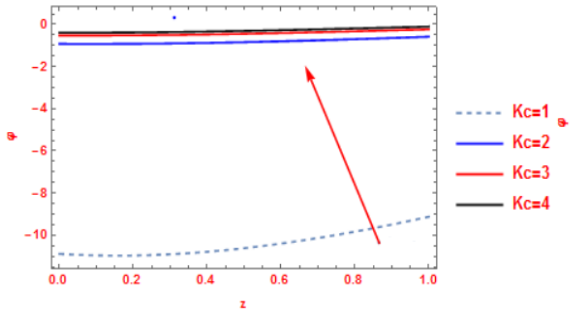

Figure 12 Concentration profile against Kc

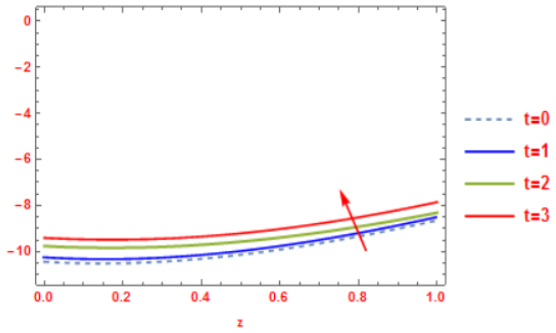

Figure 13 The concentration profile against t

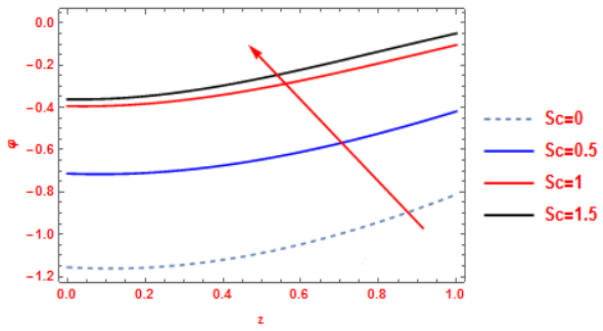

Figure 14 The concentration profile against Sc

Figure 12 that the increasing the concentration of chemical reaction (Kc) can also increase the probability that the molecules will collide with enough energy to overcome the activation energy barrier for the reaction (Kc). This is because at higher concentrations, the average distance between molecules is smaller, which means they are more likely to collide with sufficient force to initiate a reaction (Kc). Hence, increasing the concentration of reactant molecules can lead to an increase in the rate of a chemical reaction (Kc), as more collisions occur and more molecules overcome the activation energy barrier.

In a concentration profile, figure 13 that the dimensionless time (t) typically represents the time elapsed since the start of a process, divided by some characteristic time scale. As the process

progresses, more time elapses and the value of (t) increases. As the process progresses, the concentration of the substance changes and the profile evolves. The evolution of the profile can be described by the equations in terms of the dimensionless time (t). As dimensionless time (t) increases, the concentration profile changes and the concentration gradients become steeper. This is because more time has elapsed, allowing the substance to diffuse or react further. The dimensionless time (t) increases in a concentration profile because it represents the time elapsed since the start of a process, and as the process progresses, more time elapses and the value of (t) increases.

Figure 14 that the Schmidt number (Sc) is a dimensionless quantity that describes the ratio of momentum diffusivity (kinematic viscosity) to mass diffusivity in a fluid. When the concentration profile of a fluid rises, it means that there is a larger concentration gradient in the fluid. This larger concentration gradient causes a higher rate of mass transfer (diffusion) in the fluid, which in turn rises the value of mass diffusivity. Hence, the kinematic viscosity of the fluid does not change with the concentration profile. Therefore, as the value of mass diffusivity increases, the Schmidt number augments (Sc).

Micro Rotation

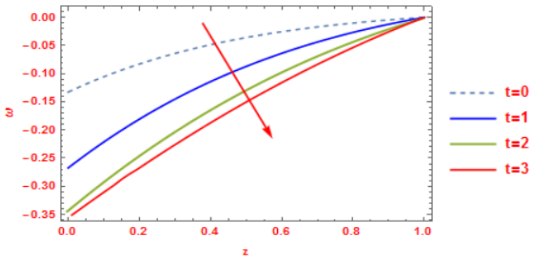

Figure 15 The micro rotation profile against t

Figure 15 that the dimensionless time (t) in the profile micro rotation typically refers to the non-dimensional time scale used to describe the fluid motion. The exact relationship between dimensionless time (t) and the micro-rotation rate will depend on the specific details of the flow being studied, but in general, as the fluid motion becomes more chaotic or turbulent, the micro-rotation rate tends to decrease with time. This is because turbulent flows tend to mix the fluid more effectively, reducing the local velocity gradients that drive micro-rotation.

Skin friction (C_f)

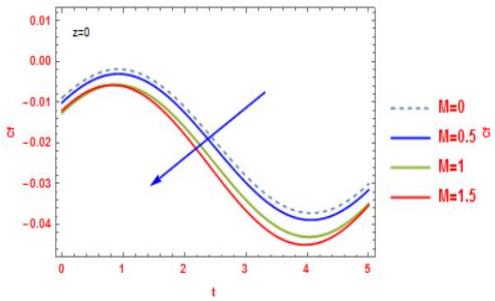

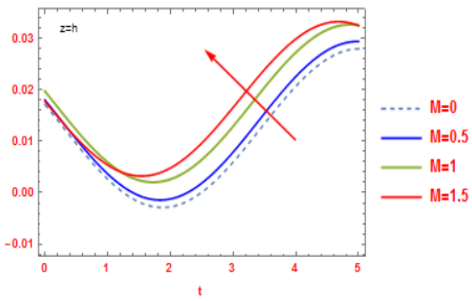

Figure 16 The Skin friction profile against M(z=0) **Figure 17 The Skin friction against M(z=h)**

In the context of skin friction (C_f), figure 16 that the Hartmann number (M) is related to the reduction of skin friction (C_f) in the presence of a magnetic field. At $z = 0$, the Hartmann number (M) decreases because the magnetic field is presumed to be inserted perpendicular to the wall, which means that the magnetic field strength lessens as the distance from the wall decreases. The reduction of skin friction (C_f) due to a magnetic field depends on the strength and orientation of the magnetic field, the velocity of the fluid, and the geometry of the flow. Therefore, the specific behaviour of the Hartmann number (M) and skin friction (C_f) at $z = 0$ will depend on the details of the particular flow and magnetic field configuration.

Figure 17 that the Hartmann number (Ha) is a dimensionless parameter that characterizes the strength of the magnetic field in a conducting fluid or plasma. the effect of a magnetic field on the skin friction (C_f) of a fluid flowing through a channel. At z=h, the skin friction (C_f) coefficient is defined as the ratio of the wall shear stress to the dynamic pressure of the fluid. While a magnetic field is inserted to the fluid flow, it can modify the skin friction (C_f) coefficient by inducing a magnetic drag force that opposes the motion of the fluid. As the Hartmann number (M) rises, the magnetic field strength increases, which leads to a stronger magnetic drag force acting on the fluid. This increased drag force results in a higher skin friction (C_f) coefficient at the wall, which is observed at z=h. Therefore, the skin friction (C_f) increases with anrise in the Hartmann number (M) at z=h.

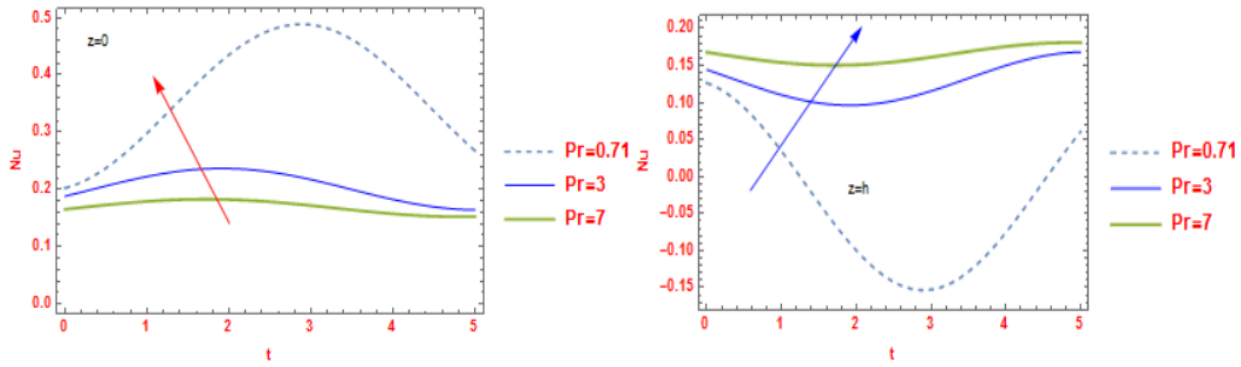

Figure 18 The Nusselt number against Pr(z=0) Figure 19 The Nusselt number against Pr(z=h)

Figure 18 shows that in the study of heat transmission, the dimensionless quantities Prandtl and Nusselt are both utilised. At $z = 0$, which usually refers to the surface of a solid object, the fluid in contact with the surface experiences a sudden change in velocity and temperature, which leads to a boundary layer formation. The boundary layer is a thin layer of fluid in contact with the solid surface, where the velocity and temperature gradients are significant. The Nusselt number (Nu) is related to the rate of heat transfer from the surface to the fluid. At the surface, the velocity and temperature gradients are high, leading to a high heat transfer rate. However, as the fluid moves away from the surface, the velocity and temperature gradients decrease, and the heat transfer rate reduces. The thickness of the boundary layer is affected by The Prandtl number (Pr). A fluid with a low Prandtl number (Pr) has a thinner boundary layer than a fluid with a high Prandtl number (Pr). Hence, at $z = 0$, the Prandtl number (Pr) decreases the Nusselt number (Nu) because a fluid with a

lower Prandtl number (Pr) has a thinner boundary layer, resulting in a higher velocity and temperature gradients and therefore a higher heat transfer rate.

Figure 19 that the relationship between the Prandtl number (Pr) and the Nusselt number (Nu) at z=h can be understood through the concept of boundary layers and the effect of viscosity on heat transfer. The boundary layer is the thin layer of fluid adjacent to a solid surface. This layer experiences a slower flow than the free stream, and its thickness is proportional to the square root of the distance from the surface. As the fluid flows over a heated surface, the temperature of the boundary layer increases, and the heat is then transferred to the rest of the fluid by conduction and convection. While the Prandtl number (Pr) is high, the heat transfer is dominated by conduction in the boundary layer, and the Nusselt number be relatively low. However, as the Prandtl number (Pr) decreases, the heat transfer is increasingly dominated by convection, and the Nusselt number (Nu)rises.

Sherwood number (Sh)

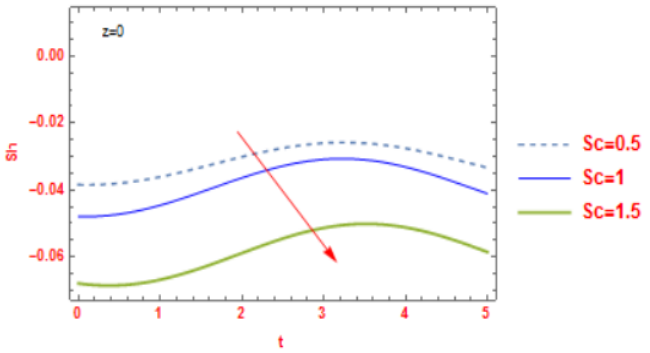

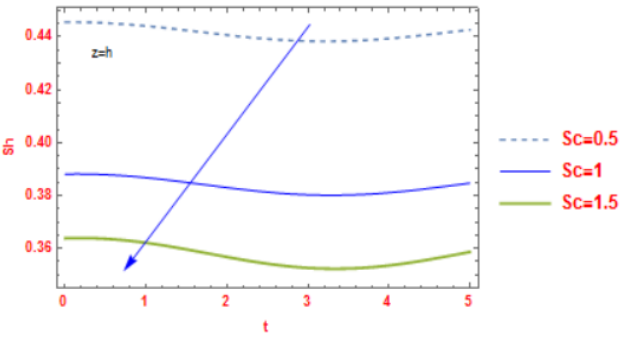

Figure 20: The Sherwood number against Sc(z=0) Figure 21: The Sherwood number against Sc(z=h)

Figure 20 that the Schmidt number (Sc) and Sherwood number (Sh) are dimensionless numbers commonly used in fluid mechanics and heat transfer. The Schmidt number (Sc) represents the ratio of momentum diffusivity (viscosity) to mass diffusivity, while the Sherwood number represents the ratio of mass transfer (diffusion) to momentum transfer (viscosity). At z=0, which is usually the reference plane, the concentration gradient is considered to be zero. This means that there is no change in concentration in the horizontal direction, and any mass transfer that occurs is due to vertical diffusion. Since the concentration gradient is small or negligible at z=0, the mass diffusivity dominates the mass transfer process, and the momentum diffusivity plays a minor role. the Schmidt number (Sc) decreases at z=0, meaning that mass diffusivity is relatively more important than momentum diffusivity. This leads to a corresponding decrease in the Sherwood number (Sh) at z=0, as the mass transfer coefficient (which is directly proportional to the Sherwood number) is primarily affected by mass diffusivity.

Figure 21 that the Schmidt number (Sc) and the Sherwood number (Sh) are both dimensionless numbers used in fluid mechanics to describe the transfer of mass or momentum in a fluid. The Schmidt number (Sc) is explained as the ratio of the kinematic viscosity of a fluid to its mass diffusivity, while the Sherwood number is defined as the ratio of the mass transfer rate to the product of the diffusivity and a characteristic length. when z=h, the Sherwood number (Sh) is describing the mass transfer behaviour of the fluid away from the wall and into the bulk flow. As the fluid moves

away from the wall, it typically experiences less resistance to mass transfer and the mass diffusivity becomes more important than the kinematic viscosity. Therefore, the Schmidt number (Sc) decreases at z=h, which causes the Sherwood number (Sh) to increase. This means that the mass transfer rate away from the wall is increasing and the fluid is mixing more efficiently. Hence, the decrease in Schmidt number (Sc) at z=h is due to the increasing importance of mass diffusivity compared to kinematic viscosity, which leads to anrise in the Sherwood number (Sh) and more efficient mixing away from the wall.

5. Conclusions

On an unsteady MHD natural convective flow of Micropolar - Casson fluid across a semi-infinite perpendicular moving porous plate using convective boundaries, the impacts of heat radiation, chemical reaction, Soret, Hall, and ion slip have been studied. The perturbation approach is utilized to solve the dimensionless governing equations. The significance of velocity, microrotation, temperature, and concentration is learned in order to identify the physical properties using the correct parameters.

The following conclusions are drawn.

- The results of the resultant velocity q, Hartmann number(M) and mass Grashof number (Gm) lessen with an increasing value. Whereas Hall parameter (α_e) increases in velocity U and decreases in velocity V with an augment value. Dimensionless time t, ion slip parameter (α_i), thermal Grashof number (Gr) and thermal radiation (N) augment with rising values.
- Furthermore, the effects of dimensionless time t exposed that increase in the temperature profile and it reduced with a mounting value in Prandtl number (Pr) and thermal radiation (N).
- Concentration profile increases with an increase in the dimensionless time t, chemical reaction (Kc) and Schmidt number (Sc).
- Microrotation profile lessens with the mounting values of dimensionless time t.
- An augment in the Hartmann number (M)and Prandtl number (Pr) at z=0 reducesthe skin friction (Cf) coefficient and Nusselt number (Nu), the reversal behaviour is detected for the skin friction coefficient and Nusselt number (Nu)while an increase in the Hartmann number (M) and Prandtl number (Pr) at z=h.Whereas Sherwood number (Sh)lessens with weaken in the increasing values of Schmidt number (Sc) at the walls z=0 and z=h.

Appendix

$$m_1 = \frac{-f_1+\sqrt{f_1^2+4f_2}}{2}; m_2 = \frac{-f_1-\sqrt{f_1^2+4f_2}}{2}; m_3 = \frac{-Sc+\sqrt{Sc^2-4f_8}}{2}; m_4 = \frac{-Sc-\sqrt{Sc^2-4f_8}}{2}; m_5 = \frac{-Sc+\sqrt{Sc^2-4f_{15}}}{2};$$

$$m_6 = \frac{-Sc-\sqrt{Sc^2-4f_{15}}}{2}; m_7 = \frac{-\delta+\sqrt{\delta^2+4in\delta}}{2}; m_8 = \frac{-\delta-\sqrt{\delta^2+4in\delta}}{2}; m_9 = \frac{-f_{31}+\sqrt{f_{31}^2-4f_{32}}}{2}; m_{10} = \frac{-f_{31}-\sqrt{f_{31}^2-4f_{32}}}{2};$$

$$m_{11} = \frac{-f_{31}+\sqrt{f_{31}^2-4f_{39}}}{2}; m_{12} = \frac{-f_{31}-\sqrt{f_{31}^2-4f_{39}}}{2}; f_1 = \frac{1}{Pr\left(1+\frac{4}{3}N'\right)}; f_2 = inf_1; f_3 = AA_1f_1^2; f_4 = -Af_1A_2f_1;$$

$$f_5 = f_1^2 + f_2; f_6 = -\frac{f_3f_1^2+f_5^2}{f_1^4+f_5^2}; f_7 = -\frac{f_5f_3-f_5f_1^2}{f_1^4+f_1^2}; f_8 = KrSc; f_9 = -ScA_1\ f_1^2; f_{10} = -A_2Scf_1^2;$$

$$f_{11} = f_8 - f_1^2; \quad f_{12} = ScD_1 - f_1^2; f_{13} = \frac{Scf_9f_1+f_{12}f_{10}}{Sc^2f_1^2+f_{12}^2}; f_{14} = -\frac{Scf_{10}f_1+f_{12}f_9}{Sc^2f_1^2+f_{12}^2};$$

$$f_{15} = Sc(Kr + in); \qquad f_{16} = -A\,ScA_5m_3; f_{17} = -A\,ScA_6m_4; \qquad f_{18} = -A\,Sc\,f_{13}f_1 - Sr\,Sc\,f_6f_1^2;$$

$$f_{19} = -A\,Sc\,f_{14}f_1 - Sr\,Sc\,f_7f_1^2; f_{20} = -Sr\,Sc\,A_3m_1^2; f_{21} = -Sr\,Sc\,A_4m_2^2; f_{22} = f_{15} - f_1^2;$$

$$f_{23}=\frac{f_{16}}{m_3^2+Sc\,m_3+f_{15}};f_{24}=\frac{f_{17}}{m_4^2+Sc\,m_4+f_{15}};f_{25}=\frac{f_{20}}{m_1^2+Sc\,m_1+f_{15}};f_{26}=\frac{f_{21}}{m_2^2+Sc\,m_2+f_{15}};f_{27}=\frac{f_{18}f_1Sc-f_{19}f_{22}}{Sc^2f_1^2+f_{22}};$$
$$f_{28}=\frac{f_{18}f_{22}+f_{19}Scf_1}{-(Sc^2f_1^2+f_{22})};f_{29}=\frac{A\,\delta}{2\,\delta-i\,n};f_{30}=\left(\frac{1+\beta c}{k}\right)+\beta r;f_{31}=\frac{1}{f_{30}};\ f_{32}=-\frac{f_{290}}{f_{30}};f_{33}=f_{32}-f_1^2;$$
$$f_{34}=\left((Gr\,A_1+Gm\,f_{14})f_{31}f_1-(GrA_2+Gmf_{13})\right)/\left(-f_{30}(f_{33}^2+f_{31}^2f_1^2)\right)$$
$$f_{35}=\left((Gr\,A_1+Gm\,f_{14})f_{33}+(GrA_2+Gmf_{13})f_{31}f_1\right)/\left(-f_{30}(f_{33}^2+f_{31}^2f_1^2)\right)$$

$$f_{36}=\frac{-Gm\,A_5}{f_{30}(m_3^2+f_{31}m_3+f_{32})};f_{37}=\frac{-Gm\,A_6}{f_{30}(m_4^2+f_{31}m_4+f_{32})};f_{38}=\frac{2\,i\,\beta_1\,\delta}{f_{30}(\delta^2-f_{31}\delta+f_{32})};f_{39}=-(i\,n+f_{290});$$
$$f_{40}=f_{39}-f_1^2;f_{41}=\frac{-A\,f_{31}m_9}{m_9^2+f_{31}m_9+f_{39}};f_{42}=\frac{-A\,f_{31}m_{10}}{m_{10}^2+f_{31}m_9+f_{39}};$$
$$f_{43}=\left(f_{31}f_1(A\,f_{31}f_{34}f_1+Gr\,f_{31}f_6+Gm\,f_{31}f_{27})+f_{40}(A\,f_{31}f_{35}f_1+Gr\,f_{31}f_7+Gm\,f_{31}f_{28})\right)/-(f_{31}^2f_1^2+f_{40}^2);$$
$$f_{44}=\left(-f_{31}f_1(A\,f_{31}f_{35}f_1+Gr\,f_{31}f_7+Gm\,f_{31}f_{28})+f_{40}(A\,f_{31}f_{34}f_1+Gr\,f_{31}f_6+Gm\,f_{31}f_{27})\right)/-(f_{31}^2f_1^2+f_{40}^2);$$
$$f_{45}=-(A\,f_{31}f_{36}m_3+Gm\,f_{31}f_{23}/m_3^2+f_{31}m_3+f_{39});$$
$$f_{46}=-(A\,f_{31}f_{37}m_4-Gm\,f_{31}f_{24}/m_4^2+f_{31}m_4+f_{39});$$
$$f_{47}=(A\,f_{31}f_{38}\delta-2i\beta_0f_{31}f_{29}\delta/\delta^2+f_{31}\,\delta+f_{39});$$

$$f_{48}=-\frac{Grf_{31}A_3+Gmf_{31}f_{25}}{m_1^2+f_{31}m_1+f_{39}};f_{49}=-\frac{Grf_{31}A_4+Gmf_{31}f_{26}}{m_2^2+f_{31}m_2+f_{39}};f_{50}=-\frac{Gmf_{31}A_7}{m_5^2+f_{31}m_5+f_{39}};f_{51}=-\frac{Gmf_3A_8}{m_6^2+f_{31}m_6+f_{39}};$$
$$f_{52}=-\frac{m_7\,2\,i\,\beta_0f_{31}}{m_7^2+f_{31}m_7+f_{39}};f_{53}=-\frac{2\,i\,\beta_0m_8}{m_8^2+f_{31}m_8+f_{39}};f_{54}=(m_{10}-\alpha f\sigma);f_{55}=(m_9-\alpha f\sigma)$$
$$;f_{56}=-f_1f_{34}-f_{36}m_3-f_{37}m_4+f_{38}\delta+(f_{35}+f_{36}+f_{37}+f_{38})\alpha f\sigma;f_{57}=e^{hm_{10}}(m_{10}+\alpha f\sigma);$$
$$f_{58}=e^{hm_9}(m_9+\alpha f\sigma);$$

$$f_{59}=-e^{hm_3}f_{36}m_3-e^{hm_4}f_{37}m_4+e^{-h\delta}\,f_{38}\delta-f_1f_{34}\cos[hf_1]+f_1f_{35}\sin[hf_1]-\alpha f\sigma\left(e^{hm_3}f_{36}+e^{hm_4}f_{37}+\right.$$
$$\left.e^{-h\delta}\,f_{38}+f_{35}\cos[hf_1]+f_{34}\sin[hf_1]\right);$$
$$f_{60}=(m_{11}-\alpha f\sigma);\qquad f_{61}=(m_{12}-\alpha f\sigma);$$
$$f_{62}=-f_1f_{43}-f_{48}m_1-f_{42}m_{10}-f_{49}m_2-f_{45}m_3-f_{46}m_4-f_{50}m_5-f_{51}m_6-f_{52}m_7-f_{53}m_8-f_{41}m_9+f_{47}\delta+$$
$$(f_{41}+f_{42}+f_{44}+f_{45}+f_{46}+f_{47}+f_{48}+f_{49}+f_{50}+f_{51}+f_{52}+f_{53})\alpha f\sigma;$$
$$f_{63}=e^{hm_{11}}(m_{11}+\alpha f\sigma);f_{64}=e^{hm_{12}}(m_{12}+\alpha f\sigma);$$
$$f_{65}=-e^{hm_1}f_{48}m_1-e^{hm_{10}}f_{42}m_{10}-e^{hm_2}f_{49}m_2-e^{hm_3}f_{45}m_3-e^{hm_4}f_{46}m_4-e^{hm_5}f_{50}m_5-e^{hm_6}f_{51}m_6-$$
$$e^{hm_7}f_{52}m_7-e^{hm_8}f_{53}m_8-e^{hm_9}f_{41}m_9+e^{-h\delta}f_{47}\delta-f_1f_{43}\cos[hf_1]+f_1f_{44}\sin[hf_1]-\alpha f\sigma\left(e^{hm_9}f_{41}+\right.$$
$$\left.e^{hm_{10}}f_{42}+e^{hm_3}f_{45}+e^{hm_4}f_{46}+e^{-h\delta}f_{47}+e^{hm_1}f_{48}+e^{hm_2}f_{49}+e^{hm_5}f_{50}+e^{hm_6}f_{51}+e^{hm_7}f_{52}+e^{hm_8}f_{53}+\right.$$
$$\left.f_{44}\cos[hf_1]+f_{43}\sin[hf_1]\right);$$
$$f_{66}=Bh\cos[hf_1]-f_1\sin[hf_1];\quad f_{67}=f_1\cos[hf_1]+Bh\sin[hf_1];$$

$$A_1=\frac{Bh\,f_1}{2\,Bh\,f_1\cos[f_1h]+Bh^2\sin[f_1h]-f_1^2\sin[f_1h]};A_2=\frac{Bh^2}{2\,Bh\,f_1\cos[hf_1]+Bh^2\sin[hf_1]-f_1^2\sin[hf_1]};$$
$$A_3=\frac{e^{m_2}(Bh\,f_6-f_1f_7)(Bh+m_2)+(-Bh+m_2)\left((Bh\,f_6+f_1f_7)\cos[f_1]+(-f_1f_6+Bh\,f_7)\sin[f_1]\right)}{e^{hm_1}(Bh+m_1)e^{hm_1}(Bh+m_1)(Bh-m_2)+e^{hm_2}(-Bh+m_1)(Bh+m_2)}$$
$$A_4=\frac{-e^{hm_1}(Bh\,f_6-f_1f_7)(Bh+m_1)+(Bh-m_1)\left((Bh\,f_6+f_1f_7)\cos[f_1]+(-f_1f_6+Bh\,f_7)\sin[f_1]\right)}{e^{hm_1}(Bh+m_1)(Bh-m_2)+e^{hm_2}(-Bh+m_1)(Bh+m_2)};$$
$$A_5=\frac{-e^{hm_4}(f_1f_{13}-Bmf_{14})(Bh+m_4)+(-Bm+m_4)(-Bh+(f_1f_{13}+Bh\,f_{14})\cos[f_1]+(Bh\,f_{13}-f_1f_{14})\sin[f_1])}{e^{hm_3}(Bh+m_3)(Bm-m_4)+e^{hm_4}(-Bm+m_3)(Bh+m_4)};$$

$$A_{10}=\frac{-\left(\left(-\left(\frac{1}{2}f_1f_{34}\,\alpha f\sigma-\frac{1}{2}f_{35}m_{10}\alpha f\sigma-\frac{1}{2}f_{36}m_{10}\alpha f\sigma-\frac{1}{2}f_{37}m_{10}\alpha f\sigma+\frac{1}{2}f_{36}m_3\alpha f\sigma+\frac{1}{2}f_{37}m_4\alpha f\sigma\right)\right)\right)}{\left(-\left(-m_{10}+e^{-h\delta}\,m_{10}+\alpha f\sigma-e^{-h\delta}\,\alpha f\sigma-\frac{1}{2}f_{38}m_{10}\alpha f\sigma-\frac{1}{2}f_{38}\alpha f\delta\sigma\right)\right)};$$
$$A_{11}=\frac{-\left(\left(-e^{-h\delta}\,f_{29}\left(-\left(-m_{10}+e^{-\delta}\,m_{10}+\alpha f\sigma-e^{-\delta}\,\alpha f\sigma-\frac{1}{2}f_{38}m_{10}\,\alpha f\sigma-\frac{1}{2}f_{38}\,\alpha f\delta\sigma\right)\right)\right)\right)}{e^{hm_8}\left(-\left(-m_{10}+e^{-h\delta}\,m_{10}+\alpha f\sigma-e^{-h\delta}\,\alpha f\sigma-\frac{1}{2}f_{38}m_{10}\,\alpha f\sigma-\frac{1}{2}f_{38}\delta\,\alpha f\sigma\right)\right)};$$
$$A_{12}=\frac{-e^{-hm_8-\delta}f_{29}+\left(e^{-m_7-m_8}\left(-e^{-h\delta}f_{29}\left(-\left(-m_{10}+e^{-\delta}m_{10}+\alpha f\sigma-e^{-\delta}\alpha f\sigma-\frac{1}{2}f_{38}m_{10}\alpha f\sigma-\frac{1}{2}f_{38}\alpha f\delta\sigma\right)\right)\right)\right)}{\left(e^{hm_8}\left(-\left(-m_{10}+e^{-h\delta}m_{10}+\alpha f\sigma-e^{-h\delta}\alpha f\sigma-\frac{1}{2}f_{38}m_{10}\,\alpha f\sigma-\frac{1}{2}f_{38}\,\alpha f\delta\sigma\right)\right)\right)};$$

$$A_{13} = \frac{\left(-e^{-hm_8-\delta} f_{29}(-2m_{12}+2\alpha f\sigma+f_1 f_{43}\alpha f\sigma-f_{53}m_{12}\alpha f\sigma+f_{53}m_8\alpha f\sigma)\right)}{((m_{11}-m_{12})\alpha f\sigma)-\frac{1}{(m_{11}-m_{12})\alpha f\sigma}};$$

$$A_{14} = \frac{\left(-e^{-hm_8-\delta} f_{29}(2m_{11}-2\alpha f\sigma-f_1 f_{43}\alpha f\sigma+f_{53}m_{11}\alpha f\sigma-f_{53}m_8\alpha f\sigma)\right)}{((m_{11}-m_{12})\alpha f\sigma)-\frac{1}{(-m_{11}+m_{12})\alpha f\sigma}};$$

$$A_{15} = -\frac{-f_1 f_{34}+f_{35}m_{10}+f_{36}m_{10}+f_{37}m_{10}-f_{36}m_3-f_{37}m_4}{m_{10}-m_9}+$$
$$\left(e^{-h\delta}\left(-2m_{10}+2e^{h\delta}m_{10}+2\alpha f\sigma-2e^{h\delta}\alpha f\sigma+e^{h\delta}f_{38}m_{10}\alpha f\sigma+e^{h\delta}f_{38}\alpha f\delta\sigma\right)\right);$$

$$A_{16} = -\frac{f_1 f_{34}+f_{36}m_3+f_{37}m_4+f_{37}m_4-f_{35}m_9-f_{36}m_9-f_{37}m_9}{m_{10}-m_9}-\left(e^{-h\delta}\left(-2m_9+2e^{h\delta}m_9+2\alpha f\sigma-2e^{h\delta}\alpha f\sigma+\right.\right.$$
$$\left.\left.e^{h\delta}f_{38}m_9\alpha f\sigma+e^{h\delta}f_{38}\alpha f\delta\sigma\right)\right);$$

$$A_6 = \frac{e^{hm_3}(f_1 f_{13}-Bm\,f_{14})(Bh+m_3)+(Bm-m_3)(-Bh+(f_1 f_{13}+Bh\,f_{14})\cos[f_1]+(Bhf_{13}-f_1 f_{14})\sin[f_1])}{e^{hm_3}(Bh+m_3)(Bm-m_4)+e^{hm_4}(-Bm+m_3)(Bh+m_4)};$$

$$A_7 = \frac{-\left(e^{hm_6}(Bm(f_{23}+f_{24}+f_{25}+f_{26}+f_{27})-f_1 f_{28}-f_{25}m_1-f_{26}m_2-f_{23}m_3-f_{24}m_4)(Bm+m_6)+(-Bm+m_6)\right)}{-e^{hm_5}(Bm+m_5)(Bm-m_6)+e^{hm_6}(Bm-m_5)(Bm+m_6)};$$

$$A_8 = \frac{\left(-e^{hm_5}(Bm(f_{23}+f_{24}+f_{25}+f_{26}+f_{27})-f_1 f_{28}-f_{25}m_1-f_{26}m_2-f_{23}m_3-f_{24}m_4)(Bm+m_5)+(Bm-m_5)\right)}{e^{hm_5}(Bm+m_5)(Bm-m_6)+e^{hm_6}(-Bm+m_5)(Bm+m_6)};$$

$$A_9 = \frac{\left(e^{-h\delta}\left(-\left(\frac{1}{2}f_1 f_{34}\,\alpha f\sigma-\frac{1}{2}f_{35}m_{10}\alpha f\sigma-\frac{1}{2}f_{36}m_{10}\,\alpha f\sigma-\frac{1}{2}f_{37}m_{10}\,\alpha f\sigma+\frac{1}{2}f_{36}m_3\,\alpha f\sigma+\frac{1}{2}f_{37}m_4\,\alpha f\sigma\right)\right)\right)}{\left(-\left(-m_{10}+e^{-h\delta}\,m_{10}+\alpha f\sigma-e^{-h\delta}\,\alpha f\sigma-\frac{1}{2}f_{38}m_{10}\,\alpha f\sigma-\frac{1}{2}f_{38}\,\alpha f\delta\sigma\right)\right)};$$

REFERENCES

[1] H. R. Kataria and H. R. Patel, “Effects of chemical reaction and heat generation/absorption on magnetohydrodynamic (MHD) Casson fluid flow over an exponentially accelerated vertical plate embedded in porous medium with ramped wall temperature and ramped surface concentration,” *Propuls. Power Res.*, vol. 8, no. 1, pp. 35–46, 2019, doi: 10.1016/j.jppr.2018.12.001.

[2] M. Veera Krishna and A. J. Chamkha, “Hall and ion slip effects on MHD rotating boundary layer flow of nanofluid past an infinite vertical plate embedded in a porous medium,” *Results Phys.*, vol. 15, no. April, 2019, doi: 10.1016/j.rinp.2019.102652.

[3] J. Sasikumar, D. Bhati, and V. Bhaskar, “Effect of heat and mass transfer on MHD oscillatory flow through asymmetric wavy channel in a porous medium with suction and injection,” *AIP Conf. Proc.*, vol. 2277, 2020, doi: 10.1063/5.0025530.

[4] A. Rahman, M. Kasim, H. Ali, and M. Al-shari, “Proceedings of the Third International Conference on Computing, Mathematics and Statistics (iCMS2017),” *Proc. Third Int. Conf. Comput. Math. Stat.*, 2019, doi: 10.1007/978-981-13-7279-7.

[5] M. G. Sobamowo, A. T. Akinshilo, and A. A. Yinusa, “Thermo-Magneto-Solutal Squeezing Flow of Nanofluid between Two Parallel Disks Embedded in a Porous Medium: Effects of Nanoparticle Geometry, Slip and Temperature Jump Conditions,” *Model. Simul. Eng.*, vol. 2018, 2018, doi: 10.1155/2018/7364634.

[6] D. Yadav and M. Maqhusi, “Influence of temperature dependent viscosity and internal heating on the onset of convection in porous enclosures saturated with viscoelastic fluid,” *Asia-Pacific J. Chem. Eng.*, vol. 15, no. 6, pp. 1–20, 2020, doi: 10.1002/apj.2514.

[7] S. I. Abdelsalam and M. M. Bhatti, “The study of non-Newtonian nanofluid with hall and ion slip effects on peristaltically induced motion in a non-uniform channel,” *RSC Adv.*, vol. 8, no. 15, pp. 7904–7915, 2018, doi: 10.1039/c7ra13188g.

[8] O. T. Bafakeeh *et al.*, “Hall Current and Soret Effects on Unsteady MHD Rotating Flow of Second-Grade Fluid through Porous Media under the Influences of Thermal Radiation and Chemical Reactions,” *Catalysts*, vol. 12, no. 10, 2022, doi: 10.3390/catal12101233.

[9] M. D. Shamshuddin and P. V. Satya Narayana, “Primary and secondary flows on unsteady MHD free convective micropolar fluid flow past an inclined plate in a rotating system: A finite element analysis,” *Fluid Dyn. Mater. Process.*, vol. 14, no. 1, pp. 57–86, 2018, doi: 10.3970/fdmp.2018.014.057.

[10] M. Veera Krishna, “Hall and ion slip effects on mhd laminar flow of an elastico-viscous (Walter’s-b) fluid,” *Heat Transf.*, vol. 49, no. 4, pp. 2311–2329, 2020, doi: 10.1002/htj.21722.

[11] M. Veera Krishna, N. Ameer Ahamad, and A. J. Chamkha, “Hall and ion slip effects on unsteady MHD free convective rotating flow through a saturated porous medium over an exponential accelerated plate,” *Alexandria Eng. J.*, vol. 59, no. 2, pp. 565–577, 2020, doi: 10.1016/j.aej.2020.01.043.

[12] M. Veera Krishna, N. Ameer Ahamad, and A. F. Aljohani, “Thermal radiation, chemical reaction, Hall and ion slip effects on MHD oscillatory rotating flow of micro-polar liquid,” *Alexandria Eng. J.*, vol. 60, no. 3, pp. 3467–3484, 2021, doi: 10.1016/j.aej.2021.02.013.

[13] D. Yadav, J. Wang, R. Bhargava, J. Lee, and H. H. Cho, “Numerical investigation of the effect of magnetic field on the onset of nanofluid convection,” *Appl. Therm. Eng.*, vol. 103, pp. 1441–1449, 2016, doi: 10.1016/j.applthermaleng.2016.05.039.

[14] M. V. Krishna and A. J. Chamkha, “Hall and ion slip effects on MHD rotating flow of elastico-viscous fluid through porous medium,” *Int. Commun. Heat Mass Transf.*, vol. 113, p. 104494, 2020, doi: 10.1016/j.icheatmasstransfer.2020.104494.

[15] D. Srinivasacharya and M. Shafeeurrahman, “Hall and ion slip effects on mixed convection flow of nanofluid between two concentric cylinders,” *J. Assoc. Arab Univ. Basic Appl. Sci.*, vol. 24, pp. 223–231, 2017, doi: 10.1016/j.jaubas.2017.03.002.

[16] D. Pal and S. Biswas, “Magnetohydrodynamic convective-radiative oscillatory flow of a chemically reactive micropolar fluid in a porous medium,” *Propuls. Power Res.*, vol. 7, no. 2, pp. 158–170, 2018, doi: 10.1016/j.jppr.2018.05.004.

[17] M. Sohail, R. Naz, and S. I. Abdelsalam, “Application of non-Fourier double diffusions theories to the boundary-layer flow of a yield stress exhibiting fluid model,” *Phys. A Stat. Mech. its Appl.*, vol. 537, p. 122753, 2020, doi: 10.1016/j.physa.2019.122753.

[18] J. K. Singh and C. T. Srinivasa, “Unsteady natural convection flow of a rotating fluid past an exponential accelerated vertical plate with Hall current, ion-slip and magnetic effect,” *Multidiscip. Model. Mater. Struct.*, vol. 14, no. 2, pp. 216–235, 2018, doi: 10.1108/MMMS-06-2017-0045.

[19] K. D. Singh, “An oscillatory hydromagnetic Couette flow in a rotating system,” *ZAMM Zeitschrift fur Angew. Math. und Mech.*, vol. 80, no. 6, pp. 429–432, 2000, doi: 10.1002/1521-4001(200006)80:6<429::AID-ZAMM429>3.0.CO;2-1.

[20] V. Aliakbar, A. Alizadeh-Pahlavan, and K. Sadeghy, “The influence of thermal radiation on MHD flow of Maxwellian fluids above stretching sheets,” *Commun. Nonlinear Sci. Numer. Simul.*, vol. 14, no. 3, pp. 779–794, 2009, doi: 10.1016/j.cnsns.2007.12.003.